Pressure Dependence of the Equilibrium Melting Temperature and Fold Surface Free Energy of *cis*-Polyisoprene

Eddy N. Dalal and Paul J. Phillips*

Department of Materials Science and Engineering, University of Utah, Salt Lake City, Utah 84112. *Received January 25, 1983*

ABSTRACT: A high-pressure hot/cold stage for optical microscopy and laser light scattering studies has been constructed by using sapphire windows. An interfacing power amplifier has permitted the stage to be used in conjunction with the Mettler FP5 control unit for precise isothermal or ramp temperature control. Accurate estimates of melting data for *cis*-polyisoprene at pressures from atmospheric to 2.6 kbar have been extrapolated to yield equilibrium melting temperatures by two independent methods that produce values in good agreement with each other. The pressure dependence of the equilibrium melting temperature may be described by the equation $T_m^\circ = 35.5 + 27.0P - 1.49P^2$. The pressure dependence of the fold surface free energy σ_e has also been evaluated, indicating a large and sudden increase in this parameter from 0.02 to 0.035 J/m^2 at a pressure approaching 1 kbar.

Introduction

In order for analyses to be made of crystallization kinetics at elevated pressures it is necessary for the variation of the equilibrium melting temperature to be known. The bulk of the information currently available is for polyethylene, and, although no formal estimation of equilibrium melting temperature variations has been made, the variation of the melting point of extended-chain crystals is known and should be a good approximation to that of the equilibrium melting temperature. There is, however, a lack of information on the pressure dependence of the melting temperature of folded-chain crystals of that polymer. It is hoped that in the long term, investigations of the pressure dependences of the melting temperatures of both folded-chain and extended-chain crystals will give information relevant to the structure of the folded-chain surface. Although many estimates of melting temperature elevation with pressure have been made, we are aware of only one previous attempt[1] to estimate the pressure dependence of any equilibrium melting temperature.

We have determined the equilibrium melting temperature T_m° of *cis*-polyisoprene at pressures ranging from atmospheric to 2.55 kbar. An optical "turbidimetric" technique was used to determine melting temperatures T_m. This technique has been discussed in an earlier paper[2] on the atmospheric-pressure value of T_m°. Greater detail, including comparison with differential scanning calorimetry and wide-angle X-ray methods, may be found in a Ph.D. dissertation.[3] Melting data have then been used to estimate the pressure dependence of the fold energy (σ_e) of crystals grown at both atmospheric and elevated pressures.

Experimental Section

The polymer (*Hevea* natural rubber) used was a grade of pale crepe supplied by the Malaysian Rubber Producers Research Association, Brickendonbury, Herts, U.K. It was Soxhlet-extracted with benzene in order to remove the stearic acid and other impurities normally present.

Equipment. Melting point measurements at high pressure were carried out by using the equipment shown in Figure 1; the numbers in square brackets refer to this figure. The high-pressure cell [1] and control attachments were mounted on a Reichert Neovar Pol microscope [2]. The microscope column had to be extended 32 mm by insertion of a rigid aluminum block, in order to provide sufficient clearance between the objective lenses and the stage carrier to accommodate the cell and attachments.

The sample could be viewed through the eyepieces, or the light beam could be switched to a photosensor [3] mounted on the phototube. The photosensor was connected to and was part of a Metrologic Radiometer 60-530 photometer [4], which provided an analog output of about 3 V full scale. This analog output was fed to a Speedomax W strip chart recorder [5] via a voltage divider.

The pumping system utilized a phosphate ester hydraulic fluid and the pressure was generated by a High Pressure Equipment Co. screw-driven hydraulic ram [6]. The system was filled from the hydraulic fluid reservoir [7] under nitrogen gas pressure. Pressure developed was measured on a Bourdon-type gage [8], and transmitted to the cell through flexible steel tubing [9].

In order to avoid ambient moisture condensation in the path of the light beam at the low temperatures (down to −20 °C) employed, it was necessary to enclose the entire microscope assembly in a glovebox [10]). Atmospheric humidity was prevented from entering the glovebox by a slow stream of dry nitrogen gas regulated by a needle valve on a flowmeter [11].

Temperature control will be discussed in detail later in this section; however, it involved a Mettler FP5 control unit [12] coupled with a specially designed interface unit [13]. Subambient cooling was achieved through the use of a Neslab RTE8 refrigerated circulating bath [14] filled with a 40 wt % solution of ethylene glycol in water. This coolant was transmitted to and from the heat exchanger on the cell in flexible Tygon tubing, insulated by a larger tube made of flexible polyurethane foam with a wall thickness of 25 mm. Coolant flow rate was regulated by an insulated bypass valve [15].

Line voltage fluctuations were found to alter significantly the output light level of the microscope. It was therefore necessary to connect the microscope to a constant-voltage transformer [16].

High-Pressure Microscopy Cell and Attachments. The high-pressure cell used in the microscopy experiments was based on a design by Daniels[4] but was heavily modified in its final form, which is shown in Figure 2; the following numbers in square brackets refer to this figure.

The primary load-bearing components were the cell body [1] and the upper [2] and the lower [3] screw plugs, which were made of VascoMax 300 CVM maraging steel, heat treated to a hardness of 52 Rockwell C.

The sample [4] was held between two polished sapphire crystals [5,6] which were in turn inserted into a short length of tight-fitting Tygon tubing [7]. One of the sapphire crystals of this assembly formed a window across the opening on the upper screw plug, while a third crystal [8] sealed the corresponding opening at the lower end. All of the sapphire crystals were 0.189 in. (4.80 mm) in diameter and 0.093 in. (2.36 mm) thick and had parallel, flat, polished faces. They were supplied by Adolf Meller Co., Providence, RI. The end crystals [5,8] were held against the corresponding polished steel surfaces at low pressures by a light helical spring [9], whose ends were ground flat and parallel. This arrangement permitted the use of samples with a range of thicknesses. Clearances between the screw plug faces and the cell body were sealed with fluorocarbon O-rings backed by steel antiextrusion rings, while a smaller O-ring prevented leakage from around the lower crystal at low pressures. The O-rings were forced into a sealing position by the brass spacers [10,11]. Hydraulic fluid was pumped into the cell through the inlet port [12].

In order to avoid upsetting the internal components (particularly the optically anisotropic sapphire crystals) while closing the cell, a nonrotating washer [13] was utilized on the lower end.

0024-9297/83/2216-1754$01.50/0 © 1983 American Chemical Society

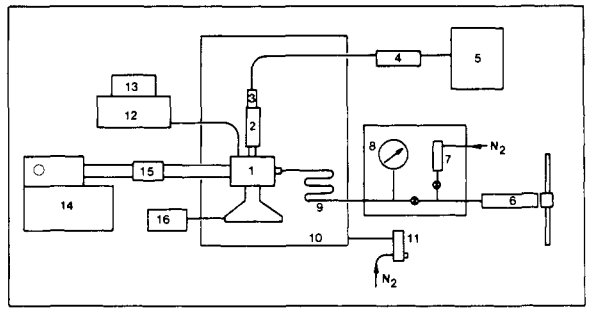

Figure 1. Equipment for high-pressure melting studies.

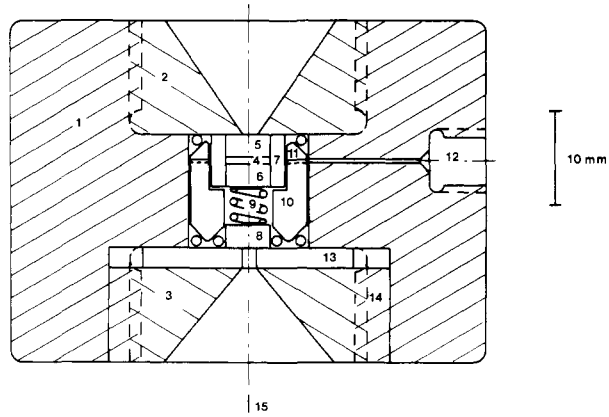

Figure 2. Sectional view of the modified high-pressure microscopy cell.

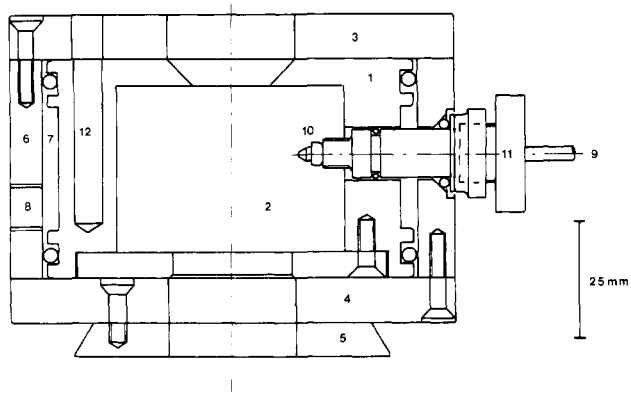

Figure 3. Sectional view of the heat exchanger.

This washer had four small radial arms that moved axially in close-fitting grooves [14] cut into the cell body. The upper surface of the washer, as well as the lower surface of the upper screw plug, was involved in direct sapphire-to-steel high-pressure seals. Hence they were ground flat and then polished with alumina (1-μm grit size) on a polishing wheel before assembly.

The light beam [15] from the microscope traveled vertically upward along the axis of the cell, passing through three sapphire crystals, the sample, and some hydraulic fluid.

Heating and cooling of the cell were achieved by means of the aluminum heat exchanger shown in Figure 3; the following numbers in square brackets refer to this figure. The aluminum body [1] of the heat exchanger enclosed a cavity [2] in which the cell fitted snugly. Thermal insulation was provided by an upper [3] and a lower [4] insulator made of reinforced phenolic resin. The aluminum base [5] was beveled so that the entire assembly could be directly fitted on the microscope in place of the rotary stage. Precise centering of the cell was possible by using the original stage-centering mechanism on the microscope.

A coaxial outer sleeve [6] made of aluminum surrounded the heat exchanger body and enclosed an annular space [7] through which a coolant could be circulated via two circulation ports [8]. Clearances between body and sleeve were sealed with O-rings. Hydraulic fluid was pumped into the cell through flexible high-

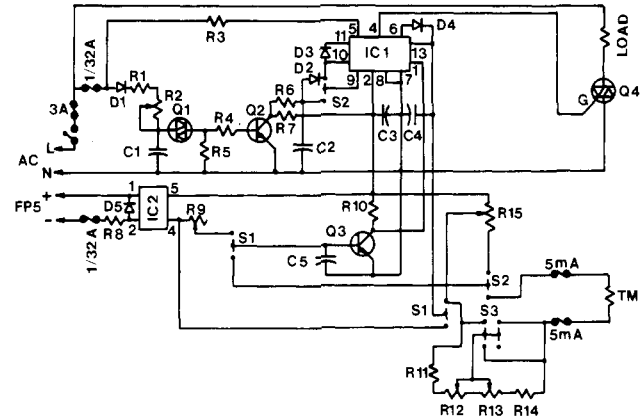

Figure 4. Circuit diagram for the interfacing power amplifier.

pressure steel tubing [9], with a shortened standard tubing collar [10] mounted on left-handed screw threads cut on the tip of the tubing. The high-pressure tubing was fastened to the inlet port of the cell by a gland nut [11] designed to carry the O-ring to seal the coolant circulation space.

Vertical cylindrical holes [12] were bored into the heat exchanger body to carry three 100-W water-resistant cartridge heaters, a thermistor probe, a platinum RTD probe, and a thermocouple probe. The heaters were the primary means of temperature control, and for set points below about 40 °C they were balanced against a regulated coolant flow that was slightly cooler. Utilization of the three probes for temperature control and measurement will be described later in this paper. The thermistor and RTD probes were fabricated from a Fenwal GB41P2 (10 kΩ) thermistor and an Instrulab 628 RTD, respectively. Each sensor was mounted in an aluminum sheath 4.76 mm in diameter and 33 mm long. The leads were insulated with PTFE sleeves and soldered to shielded low-resistance copper cables, and the assembly was potted with epoxy resin. The thermocouple was made from a length of J-type thermocouple wire sheathed in a 2.5-mm-diameter tube.

Temperature Control. Two modes of temperature control were required for melting temperature determinations. One requirement was for a constant temperature, stable over considerable lengths of time, for crystallization of the sample. The second was for temperature scanning, at a constant rate, for melting the crystals. The Mettler FP5 control unit was selected as the basis for the temperature-scanning capability. This unit has a temperature range of −20 to +300 °C, accurate to about 0.1 °C (static). Heating or cooling rates can be selected from five steps of 0.2–10 °C/min, with a linearity error of less than ±0.1 °C at the lower scan rates.

However, the Mettler FP5 unit was designed to heat a small glass microscope slide; its power output was inadequate to heat the high-pressure cell and attachments, which had enormously larger thermal masses, at the required rates. It was therefore necessary to construct an interfacing power amplifier. Zero-voltage switching practically eliminated radio-frequency interference. The maximum power output was more than 12 times that of the FP5 unit, and this could be extended as desired by triac selection. In addition, a power control feature permitted accurate balancing of the power requirements of a wide range of loads. The interfacing unit could also be used independently, without the scanning capability, as a very stable thermistor temperature controller. At the low crystallization temperatures used in these experiments, the control temperature bandwidth with the thermistor was less than ±0.01 °C, as measured by an independent thermocouple.

The circuit diagram for the interfacing power amplifier, shown in Figure 4, was based on a thermistor temperature controller designed by Granieri.[5] At the heart of this circuit was the RCA CA3509 zero-voltage switch. In the thermistor-controller mode, the interfacing unit closely resembled the original design, with minor modifications such as an arrangement for switching resistors into the circuit to extend the low-temperature range of the control potentiometer without sacrificing resolution. The nonlinear characteristics of the thermistor (Fenwal GB41P2) provided excellent temperature control at low temperatures. High-temper-

ature performance (over 80 °C) was correspondingly poor, but accurate control at such temperatures was not required in these experiments. The two 5-mA fuses on the thermistor input jack were felt to be essential because of the susceptibility of the original common-neutral circuit design to faulty supply wiring.

When switched to the power amplifier mode, the circuit was modified to replace the thermistor voltage-dividing system with a scaled output voltage from the FP5 unit. Precautions taken to protect the FP5 unit from an interfacing unit malfunction included incorporation of a 30-mM fuse and a GE 4N26 photon-coupled isolator. Detector open-circuit and short-circuit fail-safe features of the original design operated in both modes.

The platinum RTD probe (Instrulab 628) used on the heat exchanger matched the characteristics of the Mettler FP5 unit over the entire temperature range utilized. The RTD probe was connected to the male A and B terminals on the back of the FP5 unit, while the cable shield was connected to the female A terminal. The power output, used as the control input to the interfacing unit, was taken from the female D (+) and E (−) terminals.

Specimen Preparation. The purified rubber sample was first molded into a sheet of the required thickness. This was done on a hot press by using a mold made up of stainless steel platens and a 1.1-mm-thick stainless steel separator plate with a 40-mm-diameter hole cut in it. The rubber sheet was molded at 115 °C for 7 min and allowed to cool in the closed mold overnight. Significant oxidation was not anticipated since the time at high temperature was quite short and the mold was fully closed at all times.

Disks were then made from the molded sheet by using steel punches. Punching was performed in a press, with a fiberboard backing under the rubber sheet. Cooling the sheet, by wrapping it in aluminum foil and dipping into liquid nitrogen for a few seconds to bring it to a leathery state, facilitated the punching operation.

A composite tube held the sample assembly. Tygon T-3603 tubing with an inner diameter of $^3/_{16}$ in. (4.76 mm) and a wall thickness of $^1/_{16}$ in. (1.59 mm) was used, together with irradiated polyethylene shrink tubing with an inner diameter of $^3/_8$ in. (9.52 mm), a wall thickness of 0.012 in. (0.30 mm), and a maximum shrink ratio of about 2. Approximately 75-mm-long pieces of these two tubings were slipped coaxially onto a polished steel mandrel of 4.55-mm diameter and shrunk to a snug fit by heating to about 130 °C for a few seconds. Pieces of the exact length were required with smooth flat ends and were cut with an X-actoknife mounted on the tool post of a lathe. A typical length was 5.85 mm. A sapphire crystal, the rubber sample, and a second crystal were then inserted into the composite tube. To achieve optical orientation of the crystals for polarized-light applications, the second sapphire crystal was inserted halfway into the tube, held on a microscope stage, and rotated relative to the assembly until minimum transmission of cross-polarized light was obtained. The entire sample assembly was then lightly clamped and evacuated at ambient temperature for several hours to remove trapped air.

Experimental Procedure. The assembled cell was filled with the hydraulic fluid under vacuum and connected to the flexible high-pressure tubing from the pumping system. Removal of all traces of air bubbles from the cell was important in avoiding instability of the transmitted light intensity, which was quantitatively recorded. The rubber samples were periodically replaced to avoid infiltration by the hydraulic fluid. However, practically all of the samples examined were free of any such damage. Samples and their composite tube holders were not reused.

Several problems arose in the use of conventional polarized-light techniques for determination of melting points. One involved the sensitivity of the Metrologic photosensor to unpolarized low-frequency radiation; this was adequately overcome by the use of an infrared filter. Another problem involved the optically anisotropic nature of the sapphire crystals. The major problem, however, was an unexpected and large peak in polarized-light transmission at or near the melting point. This complication, presumably involving a photoelastic effect associated with melt strain, has been discussed elsewhere.[2,3]

Consequently, it was decided to run the experiments with unpolarized light, with a turbidimetric determination of the melting point. With this technique, the transmitted light intensity sharply rose (rather than fell) on melting of the crystals.[2,3] Preliminary experiments indicated no detectable difference in melting points determined by polarized- and unpolarized-light techniques. Auxiliary experiments[2,3] indicated that removal of the gel component had no detectable effect on the measured melting point.

In a typical experiment, the sample was first heated in the cell to 70 °C at atmospheric pressure (or 75 °C at 0.34 kbar for pressure runs) for 30 min to completely delete the effects of previous crystallization. This high temperature, which is about 30 °C above the *equilibrium* melting point and about 55 °C above the highest melting points observed, has been suggested by Kim and Mandelkern.[6] Preliminary experiments indicated the possibility of memory effects if lower temperatures were used.

The sample was then crystallized by applying the desired pressure and rapidly cooling the cell to the desired crystallization temperature by circulation of precooled glycol solution from the refrigerated bath. The rate of crystallization of rubber is so slow that the short period taken for this operation is not significant. Crystallization was allowed to continue for a period of 21 ± 1 h. The measured melting point of rubber crystallized at a given temperature was found to depend on the crystallization time, evidently due to isothermal thickening of the crystals. However, this effect was very small, ranging from essentially zero at the lower crystallization temperatures to about 2 °C per decade of time at the higher temperatures. This thickening process, which was studied in considerable detail at atmospheric pressure, has been discussed elsewhere.[2]

At the end of the crystallization period, the cell was heated at the chosen rate, starting from the crystallization temperature and continuing until melting was completed. The transmitted light level was continuously recorded on a strip chart recorder, with temperature marks superposed on the trace. Estimation of the melting point from the trace was discussed in a previous paper.[2]

During the isothermal crystallization process, temperature was controlled by the thermistor probe, with the interfacing unit in the thermistor-controller mode. At all other times, including the melting scan, temperature was controlled by the RTD probe and the FP5 unit, with the interfacing unit in the power amplifier mode. The thermocouple probe, with an ice reference junction and a Biddle 72-310 millivolt potentiometer, was used to set and measure the thermistor-controlled temperature and also to periodically check on the FP5-controlled temperature. The FP5 controller was found to have a zero-error of +0.6 °C, which was constant over the entire temperature range studied.

Because the temperature measurement and control were performed at the heat exchanger, the actual sample temperature while scanning had to be determined. This was done in a preliminary experiment in which a thermocouple was inserted into the middle of an actual sample, and differential readings between this thermocouple and the one on the heat exchanger were recorded under a variety of temperatures and scan rates at atmospheric pressure. Over the temperature range covered and at scan rates between 0.2 and 3 °C/min, the thermal lag between the heat exchanger and the sample was found to be fairly linear with scan rate.

$$\Delta T_{lag} = k(dT/dt) \tag{1}$$

Under isothermal conditions the lag was, of course, zero. Temperature oscillations were small on the heat exchanger, and in the sample they were virtually undetectable. The proportionality constant k was estimated to be ~1.6 min. Recorded temperatures T_{FP5} were thus corrected for zero-error and thermal lag according to

$$T = T_{FP5} - 0.6 + 1.6(dT/dt) \tag{2}$$

where temperatures were measured in °C and time was measured in minutes.

Results

Various possible melting temperature definitions from the melting traces experimentally obtained have been discussed earlier[2] for atmospheric-pressure data. With the high-pressure cell used in this work, noisy amorphous base lines were typical, presumably due to minute traces of hydraulic oil leaking onto the external sapphire windows

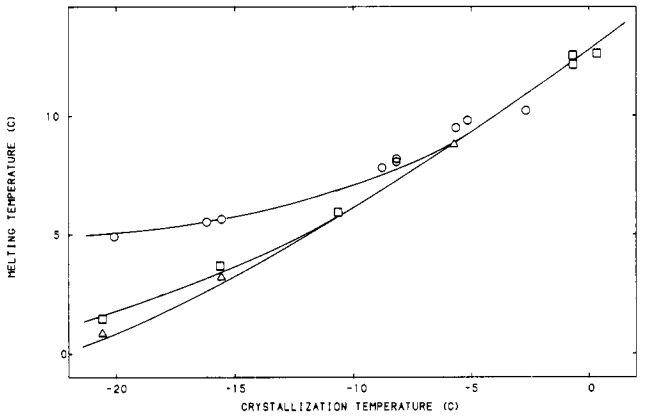

Figure 5. Comparison of atmospheric-pressure data from the FP52 stage and the high-pressure cell. The curves represent FP52 $T_{m,E}$ data from ref 2; points represent cell $T_{m,E}$ data. Heating rates: (○) 0.2, (□) 1, and (△) 3 °C/min.

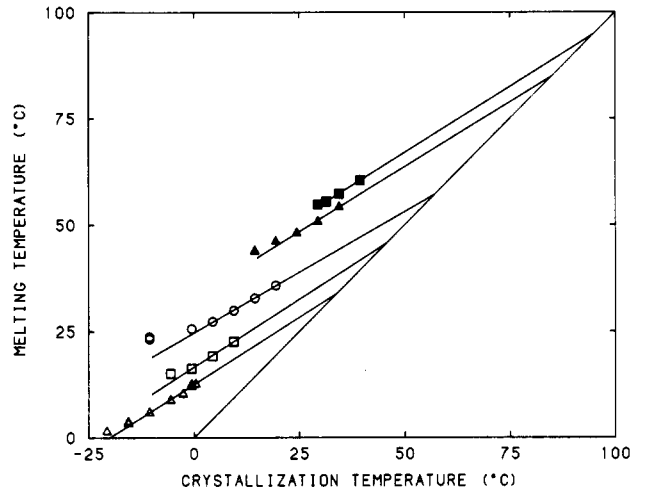

Figure 6. High-pressure melting data for material crystallized under pressure. Heating rate 1 °C/min [(△) 0.001, (□) 0.48, (○) 1.03, (▲) 2.07, and (■) 2.55 kbar].

and/or small perturbations in the position of the central, floating sapphire crystal. Consequently, the base line definition ($T_{m,B}$) of the melting temperature, which was not very sharp even with the FP52, was often so poorly defined as to be almost meaningless. In contrast, the extrapolated definition $T_{m,F}$ remained sharply defined, and therefore in this paper it will be used exclusively.

Melting temperatures reported here have been corrected by using eq 2. Crystallization time was about 21 h and unless stated otherwise, melting was carried out at a heating rate of 1 °C/min.

Quite extensive data on the melting of *cis*-polyisoprene at atmospheric pressure have been reported earlier[2,3] for an identical turbidimetric technique but carried out in the Mettler FP52 thermal microscope stage. These data are compared in Figure 5 with data obtained from the high-pressure cell used in this work. This comparison can, of course, only be carried out at atmospheric pressure. The curves in this figure represent the FP52 data,[2] for which the points have been omitted for clarity. Data from these two sources were found to be in good agreement, which is to be expected from the fact that the two procedures are essentially identical.

Figure 6 presents the melting temperatures of specimens that were crystallized and melted at pressures ranging from atmospheric to 2.55 kbar.

Extrapolation of the linear portions of each isobaric plot to the $T_m = T_c$ line yields values of $T_m°$. The lines are moved to higher T_m with increasing pressure but remain quite parallel, with slopes of about 0.6. The departure from linearity at low temperatures is evidently due to thickening during melting.

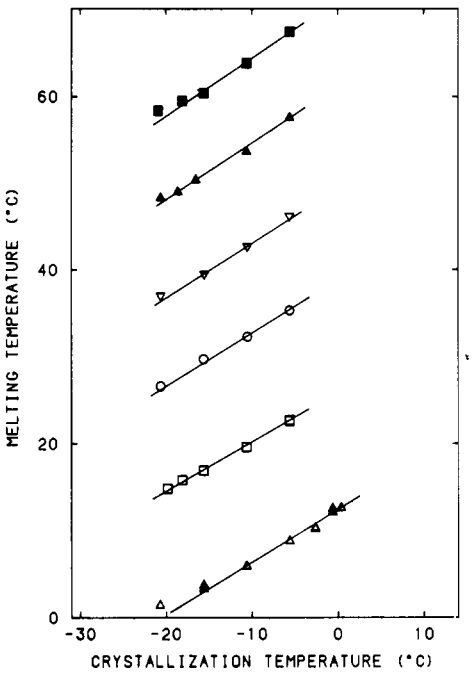

Figure 7. High-pressure melting data for material crystallized at atmospheric pressure. Heating rate 1 °C/min [(△) 0.001, (□) 0.48, (○) 1.03, (▽) 1.52, (▲) 2.07, and (■) 2.55 kbar].

Figure 7 presents equivalent data for specimens that were crystallized at atmospheric pressure and then melted at pressures ranging from atmospheric to 2.55 kbar. The plots are linear and parallel and shifted to higher temperatures with increasing pressure, as before. However, the vertical separation between the parallel isobaric plots is now almost exactly twice that of the previous case.

Extrapolation of these plots to the $T_m = T_c$ line would obviously not produce valid $T_m°$ values, because the pressure during crystallization (P_c) is not equal to the pressure during melting (P_m). Analysis of these data will be performed in the following section.

Discussion

The equilibrium melting point $T_m°$ can be obtained by two different methods. One method involves plotting T_m vs. T_c at each pressure studied, and extrapolating to intersect the $T_m = T_c$ line as illustrated in Figure 6. The extensive atmospheric-pressure data reported earlier were subjected to a somewhat more refined analysis by correcting for the δl effect.[2] The high-pressure data are not as extensive, and moreover the input parameters are not as well defined, so it was not considered meaningful to apply the δl correction to these data. It was shown in ref 2, however, that the value of $T_m°$ obtained from an uncorrected T_m vs. T_c plot is fairly close to that obtained by the corrected procedure, provided the approximately linear high-temperature end of the plot is used in the extrapolation.

The second method of determining $T_m°$ involves a plot of T_m vs. $1/l$. Since the relation between l and T_c for *cis*-polyisoprene at atmospheric pressure is well defined (see ref 2), this method can be applied by crystallizing the specimen at atmospheric pressure so that it has a known lamellar thickness, raising the pressure to the desired value, and melting the crystals under pressure. The T_m vs. T_c data presented in Figure 7 have been plotted in Figure 8 in the form of T_m vs. $1/l$. Values of l were obtained from

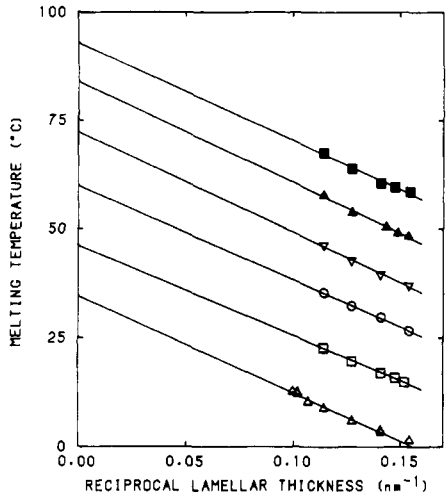

Figure 8. Plot of melting temperature against reciprocal lamellar thickness at different pressures. Material crystallized at atmospheric pressure. Heating rate 1 °C/min (symbols as in Figure 7).

Table I
Comparison of T_m° Values Determined by Two Different Methods at Pressures from Atmospheric to 2.55 kbar

pressure, kbar	T_m° (°C) from T_m vs. T_c[a]	T_m vs. $1/l$[b]
0.001	33.9	34.6
0.48	45.7	46.2
1.03	57.2	59.9
1.52		72.3
2.07	84.9	84.0
2.55	94.8	92.9
0.001[c]	35.2[c]	35.8[c]

[a] $P_c = P_m$. [b] P_c = 1 bar. [c] From ref 2.

the atmospheric-pressure T_c by the use of a second-order regression polynomial:[2]

$$l = 9.93 + 0.228T_c + 0.297 \times 10^{-2}T_c^2 \quad (3)$$

where l is in nm and T_c is in °C. The value of T_m° at each pressure is obtained by the intercept at $1/l = 0$.

Table I compares the T_m° values obtained at each pressure studied, by these two methods. These data are also plotted in Figure 9.

T_m° values from the T_m vs. $1/l$ data were found to have much less scatter than those from the T_m vs. T_c data. This is due to the relatively linear, well-defined plots obtained in the former case, which is the more reliable one because of the fewer assumptions involved.

A regression second-order polynomial was fitted to the T_m° values from the more reliable T_m vs. $1/l$ data:

$$T_m^\circ = 34.2 + 27.0P - 1.49P^2 \quad (4)$$

Here, T_m° is in °C and P is in kbar, and the correlation coefficient was 99.95%. The curve on Figure 9 plots this polynomial.

The entire set of data yielded a slightly different polynomial

$$T_m^\circ = 34.0 + 25.6P - 0.74P^2 \quad (5)$$

with a correlation coefficient of 99.78%.

The atmospheric-pressure T_m° values from ref 2, included in Table I for comparison, are about a degree higher than those calculated in this paper. The former values were obtained from extensive data at the highest heating rate (3 °C/min), using the δl correction in the case of the T_m vs. T_c data, and are considered very reliable. In addition to the fewer points in data analyzed in this paper, a slower heating rate (1 °C/min) was used to avoid considerable uncertainty in the thermal lag unavoidable with the high-pressure cell. The resultant increased thickening during melting slightly overemphasizes the low-temperature data, resulting in a lower slope and hence a lower value of T_m°. In view of these complications, the difference of a degree between the two sets of data is not excessive.

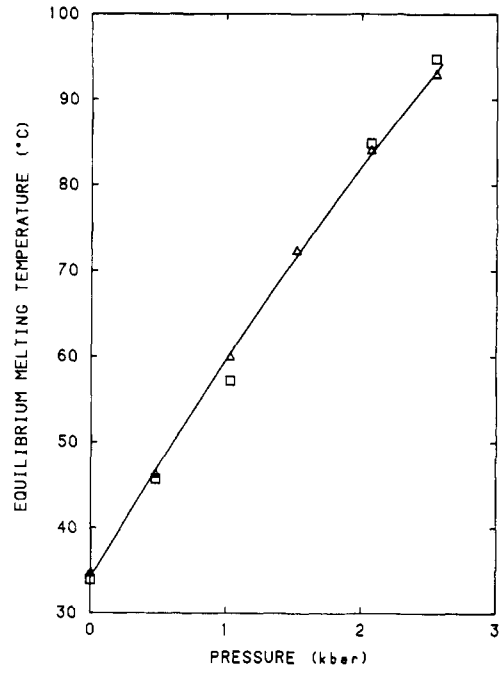

Figure 9. Variation of the equilibrium melting temperature T_m° with pressure: (△) T_m° from T_m vs. $1/l$ data, $P_c = 0$; (□) T_m° from T_m vs. T_c data, $P_c = P_m$.

Although the atmospheric-pressure T_m° data of ref 2 are more accurate, the values obtained here are used in Figure 9 as well as in the polynomials of eqs 4 and 5, so that comparisons can be made between data obtained under similar conditions. Apparently, the best estimate of the pressure dependence of T_m° would involve adding 1.3 °C to eq 4 at all pressures, leading to

$$T_m^\circ = 35.5 + 27.0P - 1.49P^2 \quad (6)$$

The initial value $(dT_m^\circ/dP)_{P=0}$ was found to be 27 °C/kbar. This can be compared with the value predicted by the Clausius–Clapeyron equation

$$\left(\frac{dP}{dT}\right)_{eq} = \frac{\Delta h_f}{T\Delta V_f} \quad (7)$$

which in this case may be written

$$\left(\frac{dT_m^\circ}{dP}\right)_{P=0} = \left(\frac{T_m^\circ \Delta V_f}{\Delta h_f}\right)_{P=0} \quad (8)$$

Taking the volume change on fusion $\Delta V_f = 1.08 \times 10^{-4}$ m^3/kg,[7] a crystalline density of 1020 kg/m^3,[8] and $\Delta h_f = 6.4 \times 10^7$ J/m^3,[6] a calculated value for $(dT_m^\circ/dP)_{P=0}$ of 53 °C/kbar was obtained. This value is twice as large as the experimental one. While these is a little uncertainty in the experimental value, there is no doubt that it is much less than 53 °C/kbar. The value of ΔV_f is reasonable when compared with the amorphous density. The only term that cannot be verified readily is the heat of fusion, a parameter that is often in dispute for common polymers. Clearly, further experimentation of a different nature is necessary to resolve this important point.

Determination of the pressure dependence of T_m° by the direct methods used here is a laborious process involving

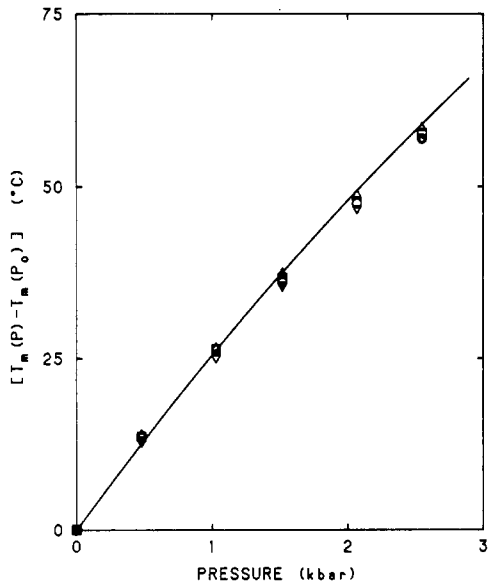

Figure 10. Melting temperature shift $T_m(P) - T_m(P°)$ for crystallization temperatures of (▲) −5.6, (□) −10.6, (○) −15.6, and (▽) −20.6 °C, in comparison with shift in equilibrium melting temperature $T_m°(P) - T_m°(P°)$, represented by the curve. Crystallization pressure P_c and reference pressure $P°$ are 1 bar.

the collection of extensive melting data at each pressure and extrapolating them. It is therefore of interest to examine whether it can be approximated by the pressure dependence of the actual melting temperature T_m of a sample crystallized at a constant temperature and atmospheric pressure and melted at various pressures.

Figure 10 presents such data for *cis*-polyisoprene, for samples crystallized at various constant temperatures. The curve in this figure represents the pressure dependence of $T_m°$, as calculated from the regression polynomials of eqs 4 or 6. Good correspondence between the pressure dependences of $T_m°$ and T_m under such conditions was found.

The data produced so far enable the pressure dependence of the fold surface free energy σ_e of the *cis*-polyisoprene folded-chain crystals to be estimated by two different methods. The first method involves the thermodynamic relationship[9] between T_m and the lamellar thickness l:

$$T_m = T_m°(1 - 2\sigma_e/\Delta h_f l) \tag{9}$$

where Δh_f is the heat of fusion per unit volume of crystal at $T_m°$.

As may be seen from this equation, σ_e can be calculated from the slopes of the isobaric plots of Figure 8, which yield the σ_e values listed in Table IIa.

Values of the heat of fusion Δh_f at each pressure, required for this calculation, are unavailable. Hence they were assumed to remain constant at the atmospheric-pressure value of 6.4×10^7 J/m^2. At least in the case of polyethylene, this is a good approximation, as seen from the work of Karasz and Jones,[10] in which Δh_f falls by no more than 2% over 1.6 kbar.

The atmospheric-pressure value of σ_e obtained in ref 2 is included in Table II for comparison. It is slightly higher than the one obtained here for the same reasons, discussed earlier, that the $T_m°$ value was slightly higher.

Values of σ_e may also be found from l vs. $1/(f\Delta T)$ data:[9]

$$l = \gamma l_g^* = \left(\frac{2\sigma_e T_m \gamma}{\Delta h_f}\right)\frac{1}{(f\Delta t)} + C_2 \tag{10}$$

where l_g^* is the initial lamellar thickness, γ is a proportionality constant, $\Delta T \equiv (T_m° - T)$ is the undercooling, and $f = 2T/(T_m° + T)$ is an empirical correction factor to account for the temperature dependence of Δh_f. This procedure was used to obtain $\sigma_e(P)$ data for specimens crystallized at high pressures. The high-pressure lamellar thickness data of Phillips and Edwards[11] were used, with $T_m°$ at each pressure calculated from the polynomial of eq 6. The corresponding plots are shown in Figure 11.

Table II

(a) Values of σ_e Obtained with Crystallization at Atmospheric Pressure from T_m vs. $1/l$ Data

P_m, kbar	σ_e, J/m^2	P_m, kbar	σ_e, J/m^2
0.001	0.0232	2.070	0.0209
0.480	0.0207	2.550	0.0198
1.030	0.0208	0.001[a]	0.0244[a]
1.520	0.0199		

(b) Values of σ_e Obtained with Crystallization at High Pressures from l vs. $1/(f\Delta T)$ Data

P_c, kbar	σ_e, J/m^2	P_c, kbar	σ_e, J/m^2
0.001[a]	0.024	2.0	0.034
0.5	0.022	2.5	0.031
1.0	0.036	3.0	0.038
1.5	0.033		

[a] From ref 2.

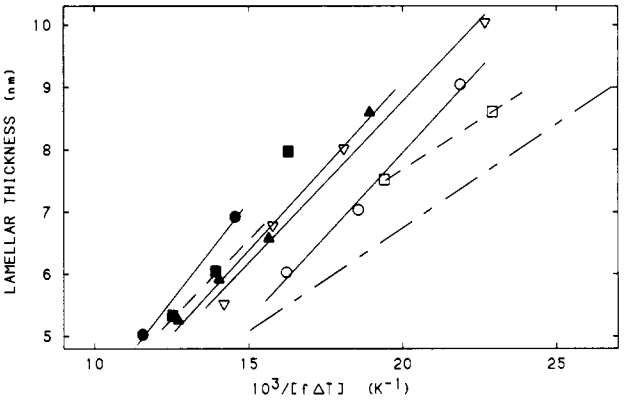

Figure 11. Plot of lamellar thickness against $10^3/(f\Delta T)$ at high pressures [(□) 0.5, (○) 1.0, (▽) 1.5, (▲) 2, (■) 2.5, and (●) 3.0 kbar]; (- - -) atmospheric pressure.

The slopes of these plots were used to find σ_e from eq 10. The heat of fusion Δh_f was again taken as 6.4×10^7 J/m^3 at all pressures. The value of γ can, in principle, be determined from a T_m vs. T_c plot.[9] However, as discussed in ref 2, it is considerably altered by the δl correction, which is not feasible with the high-pressure data for the reasons stated earlier in this paper. This necessitated the following approximation. The slopes of T_m vs. T_c plots (see Figures 6 and 7) were found to be quite constant, leading to (uncorrected) values of $\gamma \simeq 1.6$ in each case. This value was also obtained with the extensive atmospheric-pressure data of ref[2], which when subjected to the δl correction yielded $\gamma = 1.46$. This corrected value of γ was hence used at all pressures.

σ_e values obtained in this manner are listed in Table IIb. In calculating the slopes, one apparently outlying point was neglected at 1.0 and 2.5 kbar.

Values of σ_e obtained as above are compared in Figure 12. For material crystallized at atmospheric pressure and melted at high pressure, σ_e falls slightly at first and is then quite independent of pressure. On the other hand, σ_e for material crystallized at high pressure follows this same trend to 0.5 kbar, but somewhere below 1 kbar it rises discontinuously (or very steeply) to almost twice the value, at which level it remains approximately independent of

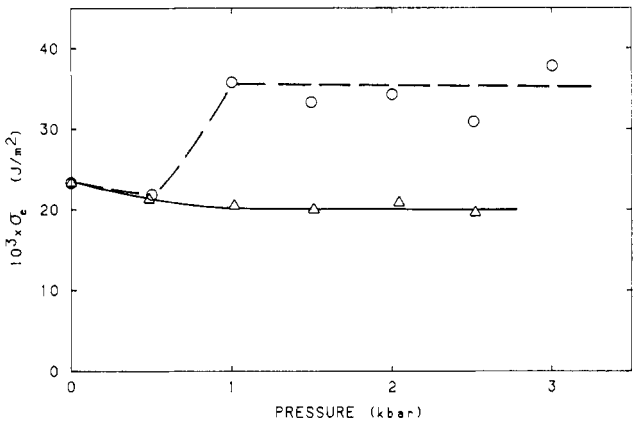

Figure 12. Pressure dependence of the fold surface free energy σ_e: (Δ) thermodynamic data (P_c = 1 bar); (O) lamellar thickness data ($P_c = P_m$).

pressure thereafter. This behavior is remarkable but is quite distinctly evident.

While σ_e data can, in principle, also be determined from T_m vs. $1/l$ data for material crystallized at high pressure, this analysis is seriously limited by practical considerations. The high-pressure lamellar thickness data available[11] is at relatively large undercoolings, in general well outside the short range of temperatures at which approximately linear T_m vs. T_c data are obtained. This eliminates a direct correlation between the melting and lamellar thickness data, and an extrapolation procedure is required. Several further approximations are needed to calculate σ_e values at high pressure, which are found to lie near 0.027 J/m^2, which is about midway between the two limiting values (0.020 and 0.035) in Figure 12. In view of the gross approximations involved, this inconclusive result is not unexpected; the increase in σ_e is nevertheless qualitatively evident.

A model involving a pressure-induced change in the crystal fold conformation has been proposed[3] to explain the behavior of σ_e at high pressure. This model will be discussed in a later publication; however, it is possible at this time to state that the observed jump is easy to reconcile with an adjacent reentry fold but does not seem to be compatible with a switchboard mode.

References and Notes

(1) C. K. L. Davies and M. C. M. Cucarella, *J. Mater. Sci.*, **15**, 1547 (1980).
(2) E. N. Dalal, K. D. Taylor, and P. J. Phillips, *Polymer*, in press.
(3) E. N. Dalal, Ph.D. Dissertation, University of Utah, 1983.
(4) W. B. Daniels, private communication.
(5) G. J. Granieri, RCA Electronic Components Manual ICAN-4158, 1969.
(6) H.-G. Kim and L. Mandelkern, *J. Polym. Sci., Part A-2*, **10**, 1125 (1972).
(7) B. Wunderlich, "Macromolecular Physics", Academic Press, New York, 1980, Vol. 3.
(8) H. Tadokoro, "Structure of Crystalline Polymers", Wiley-Interscience, New York, 1979.
(9) J. D. Hoffman, G. T. Davis, and J. I. Lauritzan, Jr., in "Treatise on Solid State Chemistry", N. B. Hannay, Ed., Plenum Press, New York, 1976, Vol. 3, Chapter 7.
(10) F. E. Karasz and L. D. Jones, *J. Phys. Chem.*, **71**, 2234 (1967).
(11) P. J. Phillips and B. C. Edwards, *J. Polym. Sci., Polym. Phys. Ed.*, **13**, 1819 (1975).

Efficient Use of Two-Dimensional Detectors for Small-Angle Neutron Scattering Contours from Polymers under External Constraint

D. F. R. Mildner

Research Reactor Facility and Department of Physics, University of Missouri, Columbia, Missouri 65211. *Received March 7, 1983*

ABSTRACT: Small-angle neutron scattering is a technique for studying polymer chain conformation using mixtures of protonated and deuterated species. When the polymer is under some external constraint, different radii of gyration are determined along directions of the scattering vector parallel and perpendicular to the stretching axis. Published experiments use only data along these two directions, and most of the data collected on two-dimensional detectors are thrown away. For a system with an axis of rotational symmetry (polymers under uniaxial stretch), the scattering cross section has elliptical symmetry at small scattering vectors. An analysis with the radius of gyration having elliptical azimuthal dependence makes efficient use of two-dimensional detectors. An elliptical fitting technique is useful particularly when part of the important data is not accessible on the spectrometer.

Amorphous polymer chains are described by random Gaussian conformation, and it is of current interest to know how this conformation changes under external constraint.[1-8] The plastic deformation behavior of polymers can be studied in two ways, isotropic deformation (e.g., swelling) or anisotropic deformation (e.g., uniaxial stretching or compression). Small-angle neutron scattering (SANS) has become a popular technique for studying the polymer chain conformation in the solid state using mixtures of protonated and deuterated species to determine the radius of gyration. The spherical averaging inherent in isotropic systems causes details in the molecular conformation to remain undetected. In highly oriented systems the conformation of the individual polymer chain depends on its orientation relative to the constraint. It is found that different radii of gyration are determined along directions of the scattering vector parallel and perpendicular to the axis of stretching or compression. The molecular theory of polymer elasticity states that the deformation is affine; that is, the dimensions of the molecular chains deform in direct proportion to the macroscopic dimensions of the sample.

SANS measurements frequently use large-area position-sensitive detectors. The intensity of scattered radiation is recorded as a two-dimensional contour (that is, as a function of scattering and azimuthal angles) representing

0024-9297/83/2216-1760$01.50/0 © 1983 American Chemical Society